Journal of the Korean Magnetic Resonance Society **2018**, *22*, 71-75
DOI 10.6564/JKMRS.2018.22.3.071

^{1}H, ^{15}N, and ^{13}C Resonance Assignments of the Anti-CRISPR AcrIIA4 from *Listeria monocytogenes* Prophages

Iktae Kim[1], Nak-Kyoon Kim[2] and Jeong-Yong Suh[1,*]

[1]Department of Agricultural Biotechnology and Research Institute of Agriculture and Life Sciences, Seoul National University, Seoul 08826, South Korea
[2]Advanced Analysis Center, Korea Institute of Science and Technology, Seoul 02796, South Korea

Received Aug 10, 2018; Revised Sep 1, 2018; Accepted Sep 5, 2018

Abstract The CRISPR-Cas system is the adaptive immune system in bacteria and archaea against invading phages or foreign plasmids. In the type II CRISPR-Cas system, an endonuclease Cas9 cleaves DNA targets of phages as directed by guide RNA comprising crRNA and tracrRNA. To avoid targeting and destruction by Cas9, phages employ anti-CRISPR (Acr) proteins that act against host bacterial immunity by inactivating the CRISPR-Cas system. Here we report the backbone ^{1}H, ^{15}N, and ^{13}C resonance assignments of AcrIIA4 that inhibits endonuclease activity of type II-A *Listeria monocytogenes* Cas9 and also *Streptococcus pyogenesis* Cas9 using triple resonance nuclear magnetic resonance spectroscopy. The secondary structures of AcrIIA4 predicted by the backbone chemical shifts show an αββββαα fold, which is used to determine the solution structure.

Keywords AcrIIA4, anti-CRISPR, Cas9, NMR spectroscopy

Introduction

The clustered regularly interspaced short palindromic repeats (CRISPR) and CRISPR-associated (Cas) proteins provide bacteria and archaea with an adaptive immunity against invading bacteriophages and foreign plasmids.[1, 2] Upon infection, the bacterial host cell activates the CRISPR-Cas system to integrate short segments (spacers) of the invading nucleic acids into the CRISPR loci. Small CRISPR RNA (crRNA) guides Cas proteins to recognize and destroy invading sequence that are complementary to the crRNA upon subsequent invasion. The CRISPR-Cas systems are grouped into two classes based on the nature of the interference complex (multiple subunits or a single subunit), and further into various types and subtypes according to the phylogeny and mechanism of action.[3] *Streptococcus pyogenes* Cas9 (SpyCas9) belongs to the subtype II-A of the Class2 CRISPR-Cas system. SpyCas9 has been extensively investigated and applied to genome editing due to its simplicity in targeting and breaking double-strand DNA at desired sites guided by single-guide RNA (sgRNA).[4-6]

Arms-race between bacteria and phages have long been evolved, developing a variety of arsenal to compete for invasion and defense.[7] Recently AcrIIA2 and AcrIIA4 encoded by *Listeria monocytogenes* prophages have shown cross-strain inhibitory effects against SpyCas9, highlighting their potential as an off-switch for Cas9 for temporal and spatial control of genome editing.[8] Biophysical and biochemical techniques have been employed to reveal the mechanism how AcrIIA4 inhibits activity of SpyCas9, such that AcrIIA4 binds to SpyCas9 via the

* Correspondence to: **Jeong-Yong Suh,** Department of Agricultural Biotechnology and Research Institute of Agriculture and Life Sciences, Seoul National University, Seoul 08826, Korea. Tel: 82-2-880-4879; E-mail: jysuh@snu.ac.kr

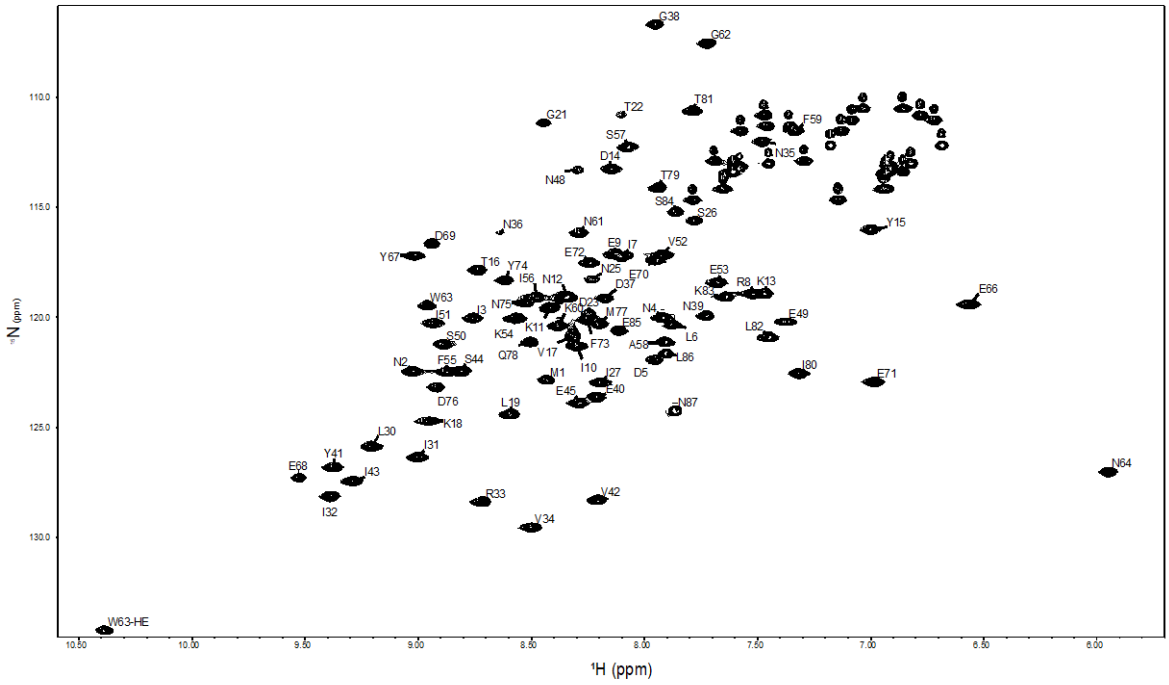

Figure 1. ^{1}H-^{15}N HSQC spectra of AcrIIA4. The backbone amide resonances are annotated with the residue types and numbers.

protospacer adjacent motif (PAM) interaction site and the RuvC domain.[9-12] Here we report the backbone chemical shifts and secondary structure of AcrIIA4 using NMR spectroscopy.

Experimental Methods

Sample preparation- The synthetic AcrIIA4 (a.a. 1–87) gene was cloned into a modified pBT7-N-His vector (ATCC) and verified by DNA sequencing. The plasmid was introduced into *Escherichia coli* strain BL21star(DE3) cells (Invitrogen), and grown minimal media with $^{15}NH_4Cl$ and/or $^{13}C_6$ glucose as sole nitrogen or carbon sources, respectively. Cells were grown at 37°C to OD_{600} ~0.8, induced with 1 mM isopropyl-β-D-thiogalactopyranoside (IPTG) at 16°C, and harvested by centrifugation after 16 hours of induction. Cell pellets were resuspended in 20 mM Tris-HCl, pH 7.4, 200 mM NaCl, 20 mM imidazole, and 1 mM phenylmethylsulfonylfluoride, lysed using Emulsiflex C3 (AVESTIN) and centrifuged at 20,000 g for 30 min. The clear supernatant was loaded onto a HisTrap column (GE Healthcare) equilibrated with 20 mM Tris-HCl, pH 7.4, 200 mM NaCl, and 20 mM imidazole, and eluted with 500 mM imidazole. The His6-tag was removed using TEV protease in 50 mM Tris-HCl, pH 8.0, 5 mM β-mercaptoethanol, and 50 mM NaCl, and the digestion reaction was loaded onto the HisTrap column. The flow-through was collected and loaded onto a Superdex 75 column (GE Healthcare) equilibrated with 20 mM Tris-HCl, pH 7.4, 200 mM NaCl. Lastly, AcrIIA4 was loaded onto a MonoQ column (GE Healthcare) and eluted with a gradient of 0.1–1 M NaCl. The purified AcrIIA4 was concentrated in 20 mM sodium phosphate, pH 7.4, 100 mM NaCl, 0.01% NaN_3

NMR experiments - The NMR sample contained 2 mM ^{13}C,^{15}N-AcrIIA4 in 20 mM sodium phosphate, pH 7.4, 100 mM NaCl, 0.01% NaN_3 and 10% D_2O. NMR spectra were recorded at 25°C on 800 MHz

spectrometers equipped with a z-shielded gradient triple resonance probe. Sequential and side chain assignments of ^{1}H, ^{15}N and ^{13}C resonances were achieved by three-dimensional triple resonance through-bond scalar correlation experiments CBCA(CO)NH, HNCACB, HNCO, HN(CA)CO, NMR spectra were processed using the NMRPipe,[13] and analyzed using PIPP,[14] and NMRView[15] programs. Overall secondary structure and the backbone dihedral torsion angles were predicted from TALOS+ based on combined HN, 15N, Cα, Cβ and CO backbone chemical shifts.[16]

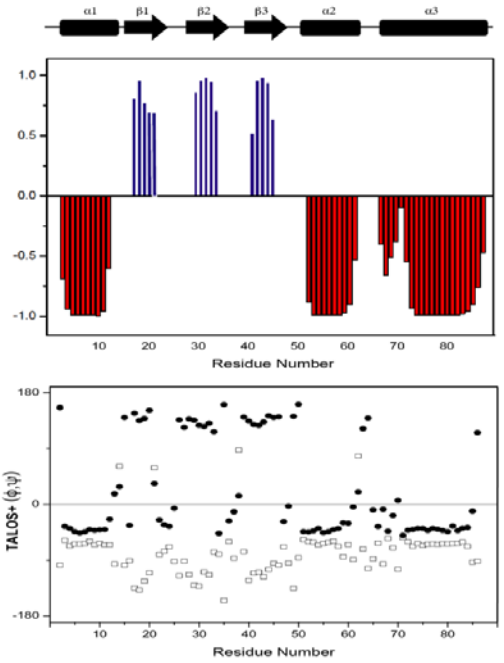

Figure 2. Predicted secondary structure (upper panel) and backbone torsion angle (lower panel) of AcrIIA4. Blue and red bar means beta-sheet and helix, respectively in the upper panel. The height of bars reflects the probability of the neural network secondary structure prediction, and schematic representations of secondary structure are displayed at the top. Backbone torsion angles (ϕ,ψ) were predicted using TALOS+ with backbone chemical shifts. Open squares and filled circles indicate phi (ϕ) and psi(ψ) angles, respectively.

Results and Discussion

Backbone assignment of AcrIIA4- AcrIIA4 consisting of 87 amino acids exhibits a well dispersed 2D [^{1}H-^{15}N]-HSQC NMR spectrum typically observed in compact folded proteins (Figure 1). The sequential backbone assignments of AcrIIA4 were performed using combinations of sets of CBCA(CO)NH with HNCACB and HNCO with HN(CA)CO using a suite of three-dimensional heteronuclear correlation NMR spectroscopy. The backbone chemical shifts were completely assigned except for Thr28 absent from backbone amide resonance in 2D ^{1}H-^{15}N HSQC spectra. Ser20, Ser24, Gln29, Glu47, and Gln65 did not show backbone amide resonances, but their aliphatic and carbonyl groups could be assigned from their sequential connectivities. ^{1}H, ^{15}N and ^{13}C assigned backbone chemical shifts of AcrIIA4 are listed in Table 1.

Secondary structure and backbone dihedral angles of AcrIIA4- Secondary structural information and backbone dihedral angles of AcrIIA4 were calculated by using TALOS+ program based on the $^{1}H_{N}$, ^{15}N, $^{13}C\alpha$, $^{13}C\beta$, and ^{13}CO chemical shifts (Fig 2). The secondary structure prediction reveled that AcrIIA4 is comprised of three α-helices and β-strands, respectively. Residue Ile3-Asn12 (α1), Ile51-Lys60 (α2), and Gln65-Ser84 (α3) constitute α-helices and Val17-Ser20 (β1), Gln29-Arg33 (β2), and Glu40-Ser44(β3) constitute the β-strands. Most of backbone dihedral angles for AcrIIA4 shows favorable phi(ϕ), psi(ψ) angles for secondary structure. The structures of AcrIIA4, revealed by X-ray crystallography and NMR spectroscopy, exhibit a same backbone fold as the predicted secondary structure derived from TALOS+.[9-12] Interestingly, the result of backbone dihedral angles shows that a loop connecting β1 and β2 is likely to short helix, and indeed in the free AcrIIA4 the loop exhibits a short 3_{10} helix required for recognition of RuvC domain of SpyCas9.[12] It also was reported that AcrIIA4 inhibits SpyCas9 by mimicking nucleotide backbone fold and implicated that loop regions of AcrIIA4 are important for recognition and binding for SpyCas9. We report backbone chemical shifts and

predicted secondary structure of AcrIIA4.

Table 1. Backbone H_N, N, Cα, Cβ, and CO chemical shifts of AcrIIA4 (unit: ppm)

Residue	HN	N	CA	CB	CO	Residue	HN	N	CA	CB	CO
M1	8.43	122.84	57.01	35.64	175.04	D37	8.17	119.14	55.23	42.12	176.54
N2	9.03	122.46	52.28	41.00	176.69	G38	7.95	106.68	46.05		174.12
I3	8.76	120.04	63.56	38.56	175.36	N39	7.73	119.93	54.46	39.02	174.47
N4	7.92	120.02	57.28	38.57	178.56	E40	8.21	123.62	55.45	33.90	174.18
D5	7.95	121.93	57.82	41.97	177.24	Y41	9.37	126.82	58.65	42.15	174.29
L6	7.88	120.34	58.99	42.04	177.86	V42	8.21	128.30	62.53	34.32	175.50
I7	8.10	117.22	67.08	38.88	177.08	I43	9.29	127.45	61.65	40.90	174.61
R8	7.52	118.93	60.46	30.48	178.90	S44	8.81	122.44	57.64	65.61	173.78
E9	8.13	117.09	59.45	30.14	179.73	E45	8.29	123.90	58.12	31.51	175.62
I10	8.30	121.32	67.39	39.73	179.08	S46	8.36	119.16	58.11	66.93	173.93
K11	8.42	119.58	60.58	32.71	181.61	E47			59.94	30.21	176.85
N12	8.34	119.06	55.59	38.83	176.64	N48	8.29	113.28	54.07	40.38	174.50
K13	7.47	118.92	55.58	32.00	174.12	E49	7.37	120.21	57.04	34.09	173.87
D14	8.15	113.25	56.74	39.18	174.85	S50	8.89	121.23	57.79	66.75	174.73
Y15	7.00	116.00	58.84	40.49	176.31	I51	8.94	120.27	66.43	38.43	177.58
T16	8.74	117.85	63.62	70.64	173.11	V52	7.92	117.14	68.01	32.63	177.47
V17	8.32	120.87	59.46	35.71	174.05	E53	7.67	118.42	60.65	30.32	180.17
K18	8.95	124.73	55.76	36.55	173.90	K54	8.56	120.04	60.58	34.05	179.29
L19	8.59	124.41	54.22	45.08	176.77	F55	8.87	122.47	62.98	40.36	176.38
S20			57.92	66.08	173.62	I56	8.48	119.09	66.00	38.52	177.97
G21	8.45	111.17	46.66		174.37	S57	8.07	112.25	62.37	63.77	177.97
T22	8.10	110.80	63.32	70.21	175.09	A58	7.91	121.13	54.70	18.61	180.48
D23	8.24	119.81	54.95	41.99	176.70	F59	7.33	111.51	59.42	40.77	178.29
S24			60.64	64.16	174.45	K60	8.38	120.39	60.41	31.66	177.23
N25	8.23	118.26	54.33	39.71	174.77	N61	8.29	116.16	53.90	39.74	175.84
S26	7.78	115.60	58.62	65.00	173.34	G62	7.72	107.54	45.94		173.62
I27	8.20	122.96	61.69	39.42	176.01	W63	8.96	119.46	59.27	29.12	175.41
T28						N64	5.95	127.04	53.22	38.17	174.41
Q29			55.73	34.36	172.62	Q65			57.57	26.18	174.68
L30	9.21	125.88	54.51	46.96	174.05	E66	6.56	119.42	60.74	30.69	176.55
I31	9.00	126.36	61.68	40.70	175.48	Y67	9.02	117.21	57.53	39.55	177.64
I32	9.39	128.13	61.43	41.88	175.48	E68	9.53	127.30	60.99	30.46	178.09
R33	8.72	128.39	57.44	30.32	175.39	D69	8.94	116.65	55.95	40.32	176.81
V34	8.50	129.56	65.53	33.05	175.77	E70	7.95	117.42	56.61	32.05	175.83

N35	7.48	112.00	52.49	40.58	175.21	E71	6.98	122.94	61.13	29.61	176.85
N36	8.64	116.15	54.83	39.13	175.46	E72	8.24	117.52	60.82	29.71	177.94
F73	8.25	120.11	61.00	39.86	177.27	T81	7.78	110.61	66.58	69.54	176.05
Y74	8.61	118.31	63.49	39.51	179.42	L82	7.45	120.92	57.23	42.52	178.68
N75	8.52	119.35	56.93	38.09	178.59	K83	7.64	119.07	58.24	32.74	177.61
D76	8.92	123.17	58.20	41.05	179.27	S84	7.86	115.21	60.56	64.72	177.62
M77	8.20	120.33	57.52	34.06	179.77	E85	8.11	120.61	57.51	30.72	176.37
Q78	8.50	121.13	60.03	28.58	180.27	L86	7.90	121.64	55.81	43.06	176.27
T79	7.94	114.11	67.31	69.41	176.61	N87	7.86	124.25	54.94	41.45	179.43
I80	7.32	122.56	66.61	38.34	178.08						

Acknowledgements

This work was supported by the Cooperative Research Program for Agriculture Science & Technology Development, Rural Development Administration (PJ013181), and the Creative-Pioneering Researchers Program through Seoul National University (500-20180204). We thank the Research Institute of Agriculture and Life Sciences, the high-field NMR facility at the Korea Institute of Science and Technology, the Korea Basic Science Institute, and the National Center for Inter-University Research Facilities.

References

1. R. Barrangou, C. Fremaux, H. Deveau, M. Richards, P. Boyaval, S. Moineau, D. A. Romero, and P. Horvath, *Science* **315**, 1709 (2007)
2. S. J. Brouns, M. M. Jore, M. Lundgren, E. R. Westra, R. J. Slijkhuis, A. P. Snijders, M. J. Dickman, K. S. Makarova, E. V. Koonin, and J. van der Oost, *Science* **321**, 960 (2008)
3. E. V. Koonin, K. S. Makarova, and F. Zhang, *Curr. Opin. Microbiol.* **37**, 67 (2017)
4. W. Jiang and L. A. Marraffini, *Annu. Rev. Microbiol.* **69**, 209 (2015)
5. S. H. Sternberg and J. A. Doudna, *Mol. Cell* **568**, 568 (2015)
6. A. V. Wright, J. K. Nunez, and J. A. Doudna, *Cell* **164**, 29 (2016)
7. J. E. Samson, A. H. Magadán, M. Sabri, and S. Moineau, *Nat. Rev. Microbiol.* **11**, 675 (2013)
8. B. J. Rauch, M. R. Silvis, J. F. Hultquist, C. S. Waters, M. J. McGregor, N. J. Krogan, and J. Bondy-Denomy, *Cell* **168**, 150 (2017)
9. D. Dong, M. Guo, S. Wang, Y. Zhu, S. Wang, Z. Xiong, J. Yang, Z. Xu, and Z. Huang, *Nature* **546**, 436 (2017)
10. H. Yang and D. J. Patel, *Mol. Cell* **67**, 117 (2017)
11. J. Shin, F. Jiang, J. J. Liu, N. L. Bray, B. J. Rauch, S. H. Baik, E. Nogales, J. Bondy-Denomy, J. E. Corn, and J. A. Doudna, *Sci. Adv.* **3**, e1701620, (2017)
12. I. Kim, M. Jeong, D. Ka, M. Han, N. K. Kim, E. Bae, and J. Y. Suh, *Sci. Rep.* **8**, 3883 (2018)
13. F. Delaglio, S. Grzesiek, G. W. Vuister, G. Zhu, J. Pfeifer, and A. Bax, *J. Biomol. NMR* **6**, 277 (1995)
14. D. S. Garrett, R. Powers, A. M. Gronenborn, and G. M. Clore, *J. Magn. Reson.* **95**, 214 (1991)
15. B. A. Johnson and R. A. Blevins, *J. Biomol. NMR* **4**, 603 (1994)
16. Y. Shen, F. Delagio, G. Cornilescu, and A. Bax, *J. Biomol. NMR* **44**, 213 (2009)